
ONEACTOR: CONSISTENT CHARACTER GENERATION VIA CLUSTER-CONDITIONED GUIDANCE

A PREPRINT

Jiahao Wang

School of Computer Science and Technology
MOEKLINNS Laboratory, Xi'an Jiaotong University
uguisu@stu.xjtu.edu.cn

Caixia Yan*

School of Computer Science and Technology
MOEKLINNS Laboratory, Xi'an Jiaotong University
yancaixia@xjtu.edu.cn

Haonan Lin

School of Computer Science and Technology
MOEKLINNS Laboratory, Xi'an Jiaotong University
linhaonan@stu.xjtu.edu.cn

Weizhan Zhang*

School of Computer Science and Technology
MOEKLINNS Laboratory, Xi'an Jiaotong University
zhangwzh@xjtu.edu.cn

ABSTRACT

Text-to-image diffusion models benefit artists with high-quality image generation. Yet its stochastic nature prevent artists from creating consistent images of the same character. Existing methods try to tackle this challenge and generate consistent content in various ways. However, they either depend on external data or require expensive tuning of the diffusion model. For this issue, we argue that a lightweight but intricate guidance is enough to function. Aiming at this, we lead the way to formalize the objective of consistent generation, derive a clustering-based score function and propose a novel paradigm, OneActor. We design a cluster-conditioned model which incorporates posterior samples to guide the denoising trajectories towards the target cluster. To overcome the overfitting challenge shared by one-shot tuning pipelines, we devise auxiliary components to simultaneously augment the tuning and regulate the inference. This technique is later verified to significantly enhance the content diversity of generated images. Comprehensive experiments show that our method outperforms a variety of baselines with satisfactory character consistency, superior prompt conformity as well as high image quality. And our method is at least 4 \times faster than tuning-based baselines. Furthermore, to our best knowledge, we first prove that the semantic space has the same interpolation property as the latent space dose. This property can serve as another promising tool for fine generation control.

1 Introduction

Text-to-image(T2I) diffusion models (Ho et al. [2020], Podell et al. [2023]) yield a significant improvement in artistic productivity. Designers can simply describe what they desire and then obtain high-quality images. In practical design scenarios, it is a necessity to maintain the consistency across images, such as the character in an animation, the product in advertising and the protagonist in a storybook. However, relying on the random sampling, traditional diffusion models fail to generate consistent images. As shown in Fig.1(a), given different "hobbit" prompts and initial noises, ordinary models generate hobbits with different identities.

As diffusion models prevail, many works try to harness the diffusion models to generate consistent content in certain extent. For example, personalization (Gal et al. [2023a], Ruiz et al. [2023], Ye et al. [2023], Wei et al. [2023]) learns to represent a new character from several given images and thus generate images of that. Storybook visualization Maharana et al. [2022], Rahman et al. [2023] manages to generate consistent characters throughout a story. However, they require external data to function, either a given image set or a specific storybook dataset. Such a requirement makes the practical usage cumbersome. Also, they are unable to illustrate imaginary, fictional or novel characters.

*Corrsponding authors.

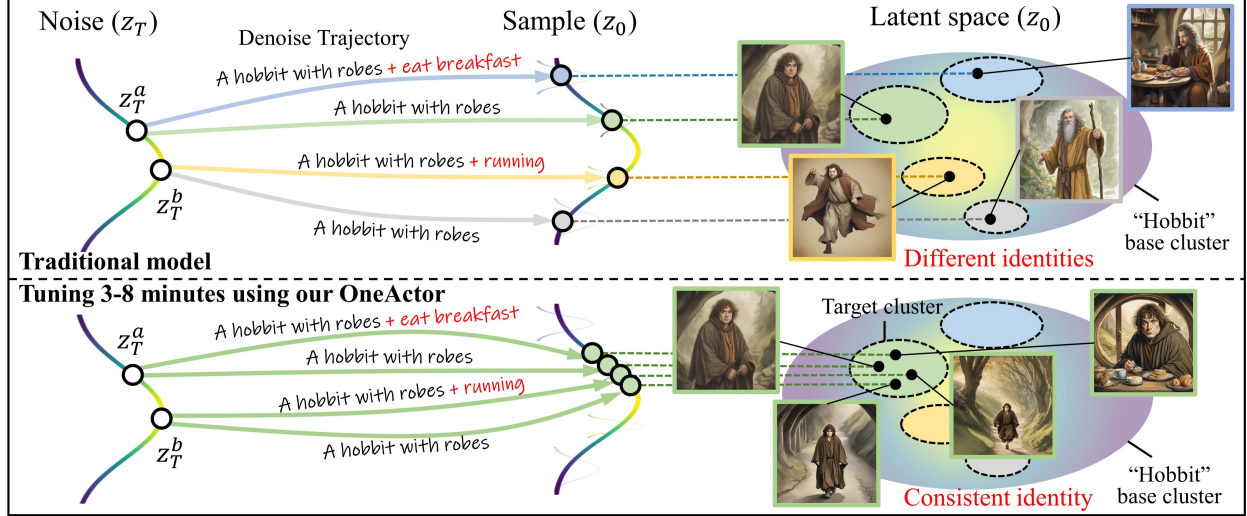


Figure 1: The illustration of the effect of our OneActor. (a) Given different "hobbit" prompts and initial noises, ordinary models generate inconsistent images from different identity sub-clusters of the concept "hobbit" cluster. (b) While our OneActor, after a quick tuning, is able to generate images from the target sub-cluster that show a specific identity. Different colors denote different identity clusters.

More recently, TheChosenOne (Avrahami et al. [2023a]) addresses a new task, consistent character generation, which aims to generate consistent images of the same character only driven by prompts. Thus, it gets rid of the requirement of the external data. And artists can easily describe the character and start their creation, which is a more intuitive manner. To accomplish this task, they generate image proposals, find the most cohesive cluster of the proposals and perform personalization tuning. Because they repeat the process until convergence, this pipeline is tedious with an average time of 20 minutes. Besides, artists have to wait for the whole process to have a glimpse of the character. If they are not satisfied with the character and want to recreate, they have to wait all over again.

In fact, diffusion model can generate two consistent images with a low probability, which indicates that they are inherently potential for consistent generation. Based on this fact, we assume that in the latent space of a pre-trained diffusion model, samples of different concepts form different clusters, i.e. *base cluster*. In a specific base cluster, samples that share common appearance gather into the same cluster, i.e. *identity sub-cluster*. As illustrated in Fig.1, for example, a "hobbit" base cluster contains four different identity sub-clusters. We argue that all the original model needs is a lightweight but intricate guidance to tame their potential. Thus, instead of confining it to the same sub-cluster as TheChosenOne does, we aim to make full use of its inner capacity and carefully guide it to find the intrinsic consistent trajectories.

To this end, we propose a novel one-shot tuning paradigm, termed as OneActor, and perform this task $4\times$ faster. In our concise paradigm, artists describe the needed character and choose one satisfactory image from the generated proposals as the target. Then, after a quick tuning of 5 minutes, as shown in Fig1(b) our OneActor quickly learns to find the denoising trajectories towards the target sub-cluster, generating images of the same character.

More concretely, to perform the cluster-guided generation, we first formalize the consistent generation task in the mathematical expression and derive the cluster-based score function. Then, to implement this function, we construct a cluster-conditioned model, which introduces the generated samples as the cluster representation. This representation is then transformed into a semantic offset by a projector. We only tune the projector to avoid harming the capacity of the denoising network or changing the structure of the latent space. Also, we approximate and simplify the function to accelerate the tuning. Finally, for better generation quality, we prove the interpolation property of the semantic space and utilize it in the inference process.

Comprehensive experiments are carried out to prove the effectiveness of our method. In terms of character consistency and prompt conformity, our OneActor form a new Pareto front over the baselines. The user study also shows our superiority over the baselines from a human perspective. Meanwhile, our OneActor only requires 3-8 minutes to tune, which is at least four times faster than tuning-based baselines.

2 Related Work

Consistent Text-to-Image Generation. A variety of works aim to overcome the randomness challenge of the diffusion models. To start with, *personalization*, given several user-provided images of a character, aims to generate consistent images of the same character. To perform this task, Gal et al. [2023a], Vinker et al. [2023] optimize a semantic token to represent the character, while Ruiz et al. [2023], Avrahami et al. [2023b] tune the entire diffusion model to learn the distribution of the given character. Later, Alaluf et al. [2023], Han et al. [2023], Kumari et al. [2023], Tewel et al. [2023] find that tuning partial parameters of the diffusion model is effective enough. Apart from the tuning-based methods above, Gal et al. [2023b], Chen et al. [2023], Arar et al. [2023], Ye et al. [2023], Wei et al. [2023] propose encoder-based methods, which carefully encode the given character into a representation without tuning. However, depending on external given images, they fail to generate imaginary or novel characters. Recently, Avrahami et al. [2023a] set up a new task, *consistent character generation*, which aims to generate images of one character given only its descriptive prompts. Though, their tuning of the whole diffusion model is expensive and may degrade the generation quality. To this end, we formalize the consistent generation, derive a cluster-based score function and design a new cluster-guided paradigm which only tunes a lightweight projector instead of the whole model.

Semantic Control of Text-to-Image Models. Ho and Salimans [2022] first propose a text-conditioned denoising network to perform text-to-image generation. They introduce a semantic space and entangle it with the latent space. Thus, the text prompt can guide the denoising trajectory towards the expected destination. Since then, many works manage to manipulate the semantic space to accomplish various tasks. For personalization, Gal et al. [2023a] learn an extra semantic token to guide the latent to the character cluster, while Zhang et al. [2024] push the token embedding to its core distribution to alleviate the overfitting. For image editing, Parmar et al. [2023], Nguyen et al. [2023] calculate a residual semantic embedding to indicate the editing direction. These works repeatedly confirm that manipulating the semantic space is an effective way to harness diffusion models for various goals. Hence, for the consistent generation, we introduce the cluster condition and transform it into a semantic representation. The representation will guide the latent to the corresponding cluster.

3 Preliminaries

Before introducing our method, we first give a brief review of basic text-to-image diffusion models. To start with, Gaussian diffusion models (Sohl-Dickstein et al. [2015], Ho et al. [2020]) assume a forward Markov process that gradually adds noise to normal image:

$$x_t = \sqrt{\bar{\alpha}_t} x_0 + \sqrt{1 - \bar{\alpha}_t} \epsilon_t, \quad (1)$$

where $t \in [0, T]$, $\bar{\alpha}_t$ are a set of constants. Meanwhile, a denoising network ϵ_θ , usually a U-Net (Ronneberger et al. [2015]), is trained to reverse the forward process by estimating the noise given a corrupted image:

$$\mathcal{L}(\theta) = \mathbb{E}_{t \in [1, T], x_0, \epsilon_t} [\|\epsilon_t - \epsilon_\theta(x_t, t)\|^2]. \quad (2)$$

Once trained, we can sample images x_0 with ϵ_θ from a Gaussian noise x_T by gradually removing the noise step by step. To introduce conditional control, classifier-free guidance (Ho and Salimans [2022]) trains ϵ_θ in both unconditional and conditional manners: $\epsilon_\theta(x_t, t, c_\emptyset)$ and $\epsilon_\theta(x_t, t, c)$, where c is the given condition and c_\emptyset indicates no condition. Images are then sampled by the combination of two types of outputs:

$$\epsilon_\theta(x_t, t, c_\emptyset) + s \cdot (\epsilon_\theta(x_t, t, c) - \epsilon_\theta(x_t, t, c_\emptyset)), \quad (3)$$

where s is the guidance scale. To accelerate the pipeline, latent diffusion models (Rombach et al. [2022]) pre-train an autoencoder to compress images into latent codes: $z = E_a(x)$, $x = D_a(z)$. Thus, the whole diffusion process can be carried out in the latent space instead of the salient image space.

4 Method

4.1 Problem Definition

Given a user-defined description prompt p^{tar} (e.g. *a hobbit with robes*), a standard diffusion model ϵ_θ generates a user-preferred image x^{tar} as the target character. Our goal is to equip the original ϵ_θ with a supportive network ϕ , formulating $\epsilon_{\theta, \phi}$. After a quick tuning of ϕ , our model $\epsilon_{\theta, \phi}$ can generate consistent images of the same character with any other character-centric prompt (e.g. *a hobbit with robes + walking on the street*).

To accomplish this task, We first give mathematical analysis in Sec.4.2. Then we construct a cluster-conditioned model in Sec.4.3, which is a self-guided diffusion model. We tune it in a contrastive manner in Sec.4.4. Finally during inference, we generate diverse consistent images with semantic interpolation in Sec.4.5 and latent guidance in Sec.4.6.

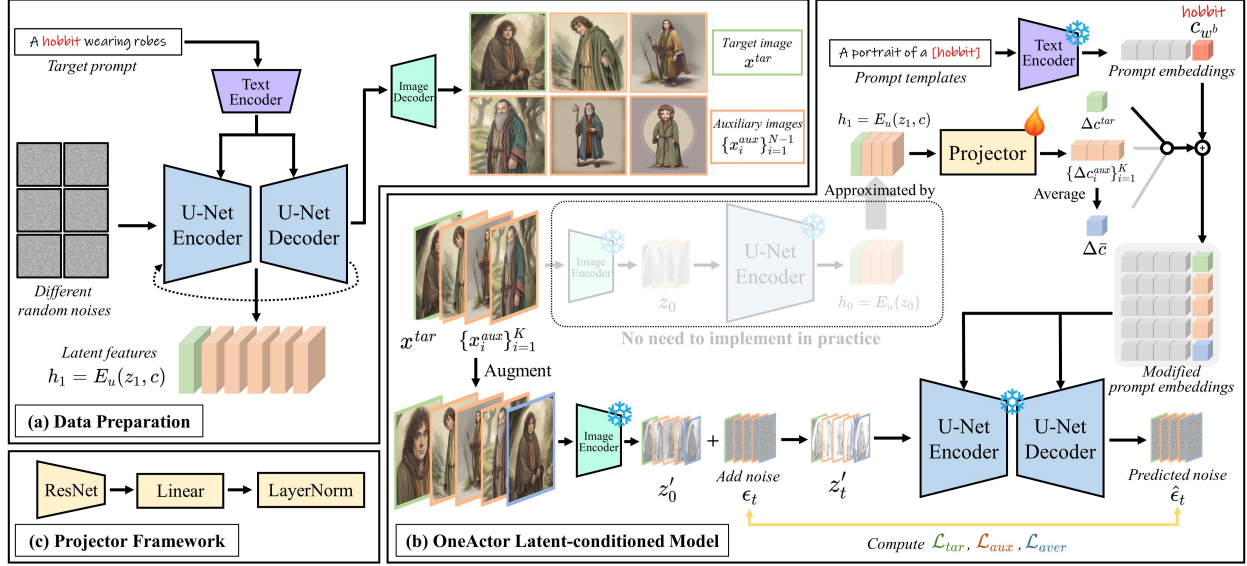


Figure 2: The overall architecture of the proposed OneActor. (a) We first generate base images and divide them into target and auxiliary set. (b) We construct a latent-conditioned model and tune the projector with batched data. (c) The projector consists of ResNet network, linear and LayerNorm layers. Tuning and freezing weights are denoted by fire and snowflake marks. The items used to compute different objectives are outlined in different colors. The unimplemented theoretical models are semi-transparent.

4.2 Derivation of Cluster-Guided Score Function

Given a user-defined prompt p^{tar} (e.g. *a beautiful girl with white dress*) and the corresponding base word w^b (e.g. *girl*), we input p^{tar} into standard diffusion models to obtain N base images $\mathcal{X}^{\text{base}} = \{x_i^{\text{base}}\}_{i=1}^N$. We randomly choose one image as the target character x^{tar} and denote the others as auxiliary samples $\mathcal{X}^{\text{aux}} = \{x_i^{\text{aux}}\}_{i=1}^{N-1}$. We apply face crop and image flip to target image for an augmented set $\mathcal{X}^{\text{tar}} = \{x_i^{\text{tar}}\}_{i=1}^M$.

In a standard latent diffusion model $\epsilon_\theta(z_t, t, c)$, for text control, conditions c are generated by a text encoder E_t , which projects text prompts p into semantic vectors: $c = E_t(p)$. These semantic vectors then guide the denoise network to sample the denoised z_0 from the initial latent noise z_T . In our task, we assume that in the latent space of z_0 , there are different clusters that correspond to different salient identities of characters. Given different initial z_T and the same character condition p^{tar} , ϵ_θ fails to reach one specific cluster, but spreads to a region of different clusters. That is to say, the generation of $\mathcal{X}^{\text{base}}$ forms a base region S^{base} , which includes one target cluster and several auxiliary clusters: $S^{\text{base}} \supset S_1^{\text{tar}} \cup S_1^{\text{aux}} \cup S_2^{\text{aux}} \cup \dots$. The key to consistent generation is how to guide ϵ_θ to the expected target cluster S^{tar} .

To start with, we formalize the consistent generation problem. From a result-oriented perspective, we expect to increase the probability of generating images of the target cluster S^{tar} and reduce that of the auxiliary clusters S_i^{aux} . Thus, if we consider the original diffusion process as a prior distribution $p(x)$, our expected distribution can be denoted as:

$$p(x) \cdot \frac{p(S^{\text{tar}} | x)^{\eta_1}}{\prod_{i=1}^{N-1} p(S_i^{\text{aux}} | x)^{\eta_2}}, \quad (4)$$

where η_1, η_2 are scale power factors. We apply the Bayes Rule to derive:

$$p(x) \cdot \frac{\left(\frac{p(x|S^{\text{tar}})p(S^{\text{tar}})}{p(x)} \right)^{\eta_1}}{\prod_{i=1}^{N-1} \left(\frac{p(x|S_i^{\text{aux}})p(S_i^{\text{aux}})}{p(x)} \right)^{\eta_2}}, \quad (5)$$

We further take its gradient of the log probability and ignore irrelevant terms to obtain:

$$\nabla \log p(x) + \eta_1 \cdot [\nabla \log p(x | S^{\text{tar}}) - \nabla \log p(x)] - \eta_2 \cdot \sum_{i=1}^{N-1} [\nabla \log p(x | S_i^{\text{aux}}) - \nabla \log p(x)]. \quad (6)$$

If we introduce the concept of score function (Song et al. [2021]), each term in Eq.6 represents a score and guides the inference process. With the reparameterization trick of (Ho et al. [2020]), we can express the scores as the predictions

of the denoising network θ in the latent space:

$$\epsilon_{\theta}(z_t, t) + \eta_1 \cdot [\epsilon_{\theta}(z_t, t, S^{tar}) - \epsilon_{\theta}(z_t, t)] - \eta_2 \cdot \sum_{i=1}^{N-1} [\epsilon_{\theta}(z_t, t, S_i^{aux}) - \epsilon_{\theta}(z_t, t)]. \quad (7)$$

This formula, termed as *cluster-guided score function*, is the core of our work. We will manage to realize it in our subsequent parts.

4.3 Cluster-Conditioned Model Using Semantic Representation

According to Eq.7, we need to introduce the cluster representations to our pipeline and build up a cluster-conditioned model $\epsilon_{\theta}(z_t, t, S)$. To this end, we regard the latent codes of the samples as the cluster representations and construct ϕ as an encoder. As shown in Fig.2, it takes the latent code z as input and outputs a character-specific vector Δc . This vector represents the semantic direction of the character cluster. Given a text prompt p , we split the prompt embeddings into word-wise embeddings: $c = \{c_{w_i}\}$, where w_i is the i -th word of the prompt. We locate the base word embedding c_{w_b} and offset it with the output vector:

$$c'_{w_b} = c_{w_b} + \Delta c. \quad (8)$$

Intuitively, ϕ acts like the text encoder and projects the latent codes into semantic embeddings. So we term ϕ as a latent encoder. The latent encoder consists of an extractor and a projector. Since the original U-Net encoder E_u is already well-trained to extract features from the latent samples, we use it directly as the extractor. The projector is a multi-layer ResNet (He et al. [2016]) and linear network with layer normalization. During tuning, we only fire the projector and freeze all other components.

However, the U-Net extractor may cause extra computational burden. So to simplify, we approximate the features of z_0 with that of z_1 :

$$h = E_u(z_1, c) \approx E_u(z_0). \quad (9)$$

Thus, when generating base images, we save the outputs $\mathcal{H} = \{h_i\}_{i=1}^N$ of the U-Net encoder in the last sampling step. h can be approximated as the output of the extractor. During tuning and inference, h is directly fed into the projector: $\Delta c = \phi(h)$. With this approximation, we avoid the extra computation of U-Net extractor and reduce the computational cost by 30%.

By now, all the factors (i.e. p, h) that could determine a cluster can be processed by the text encoder and the latent encoder. So we can express the cluster-conditioned terms in Eq.7 as:

$$\epsilon_{\theta}(z_t, t, S) = \epsilon_{\theta, \phi}(z_t, t, E_t(p), \phi(h)). \quad (10)$$

4.4 Generalized and Simplified Tuning with Auxiliary Samples

In the tuning process of our cluster-conditioned model, the intrinsic property of diffusion models is the key aspect. We aim to take full advantage of the target and auxiliary samples to: balance and stabilize the projector.

The major challenge in one-shot tuning is overfitting. The insufficiency of data may lead to severe bias and limited diversity of generated images. To overcome this challenge, we tune the model with not only target samples, but also auxiliary samples. Specifically, we randomly select 1 target and K auxiliary samples to form a batch of data: $\mathcal{B} = \{x^{tar}, h^{tar}\} \cup \{x_i^{aux}, h_i^{aux}\}_{i=1}^K$. Thus, more data contributes to the optimization and the batch normalization can be applied to the projector, resulting in a more generalized projection. For the tuning pipeline, We first get the latent codes by: $z = E_a(x)$, $x \in \mathcal{B}$ and add noise ϵ_t to them. Then as shown in Fig., we input the noisy latent z_t , prompt p and feature h to the cluster-conditioned model. The prompt is a random template filled with the base word (e.g. *a portrait of a girl*). We apply the standard denoising loss for both target and auxiliary samples:

$$\mathcal{L}_{tar}(\phi) = \mathbb{E}_{t \in [1, T], z_0^{tar}, \epsilon_t} [\|\epsilon_t - \epsilon_{\theta, \phi}(z_t^{tar}, t, E_t(p), \phi(h^{tar}))\|^2], \quad (11)$$

$$\mathcal{L}_{aux}(\phi) = \mathbb{E}_{t \in [1, T], z_0^{aux}, \epsilon_t} [\|\epsilon_t - \epsilon_{\theta, \phi}(z_t^{aux}, t, E_t(p), \phi(h^{aux}))\|^2]. \quad (12)$$

For the auxiliary term in Eq.7, it's laborious to calculate the denoising predictions of $N - 1$ auxiliary conditions for every step. To simplify, we propose an average condition $\Delta \bar{c}$. It is derived by averaging the condition vectors of the auxiliary:

$$\Delta \bar{c} = \frac{1}{K} \sum_{i=1}^K \Delta c_i^{aux} = \frac{1}{K} \sum_{i=1}^K \phi(h_i^{aux}). \quad (13)$$

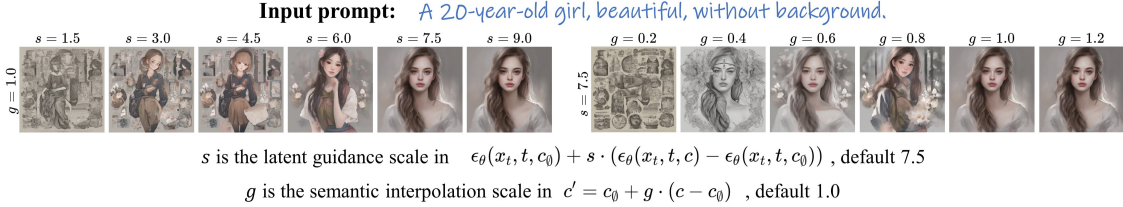


Figure 3: The observation of the effect of semantic interpolation. We vary the semantic interpolation scale in the first line and the latent guidance scale in the second line, respectively. The semantic and latent manipulations show the same effect, which proves our argument.

Intuitively, this average condition indicates the center of all the auxiliary clusters. Thus, the auxiliary denoising predictions can be approximated with this one average prediction. The denoising loss is also used in this condition:

$$\mathcal{L}_{aver}(\phi) = \mathbb{E}_{t \in [1, T], z_0^{tar}, \epsilon_t} [\|\epsilon_t - \epsilon_{\theta, \phi}(z_t^{tar}, t, E_t(p), \Delta \bar{c})\|^2]. \quad (14)$$

Note that the data here is from target set. This average condition will act as the empty condition of classifier-free guidance (Ho and Salimans [2022]) later in Sec.4.6. Thus, the complete tuning objective consists of the above 3 losses:

$$\mathcal{L}(\phi) = \mathcal{L}^{tar}(\phi) + \lambda_1 \mathcal{L}^{aux}(\phi) + \lambda_2 \mathcal{L}^{aver}(\phi), \quad (15)$$

where λ_1, λ_2 are weight hyper-parameters.

4.5 Proof and Implementation of Semantic Interpolation

During inference, traditional tuning-based pipelines share the same imbalance between consistency and diversity. To solve this problem, we suggest a mild strategy, semantic interpolation, which utilizes the internal capacity of diffusion models.

Classifier-free guidance models (Ho and Salimans [2022]) prove that the conditional interpolation and extrapolation in the latent space reflect the same linear effect in the image space. That is to say, when we increase the guidance scale s in Eq.3 within a proper range, the generated image will be more and more compliant with the prompt, as shown in Fig.3.

We argue that the semantic space of the prompt also shares this property. To prove it, we carry out experiments on SDXL (Podell et al. [2023]). In practice, empty condition c_\emptyset is also a semantic embedding obtained by encoding an empty string. So we perform interpolation in semantic space: $c' = c_\emptyset + g \cdot (c - c_\emptyset)$. Then we replace c with c' in the standard diffusion process. Fig.3 illustrates the results. With g increasing, we can observe the same liner reflection in the image space, just as that caused by the latent interpolation. It proves that the semantic space also demonstrates the ability of interpolation. We believe that this is because the semantic and latent space are entangled by the denoising network. So they share some properties in common.

With this key observation, we can precisely control the effect of Δc . Concretely, we replace the Eq.8 with:

$$c'_{w^b} = c_{w^b} + v \cdot \Delta c, \quad (16)$$

where v is the semantic scale that can be modified. Larger v leads to better consistency, while smaller leads to better diversity. Since we never harm the capacity of the original denoising network, a moderate v that leads to a optimal balance of consistency and diversity can be found.

4.6 Inference with Cluster-Guided Score Function

After tuning, we obtain an optimal ϕ^* . In the inference process, we utilize it to pave a way towards the target cluster and away from the auxiliary clusters.

During inference, with the cluster-conditioned model in Sec.4.3 and the average condition in Sec.4.4, the Eq.7 can be transformed into:

$$\begin{aligned} & \epsilon_\theta(z_t, t, \emptyset) + \eta_1 \cdot [\epsilon_{\theta, \phi^*}(z_t, t, E_t(p), \phi^*(h^{tar})) - \epsilon_\theta(z_t, t, \emptyset)] \\ & - \eta_2 \cdot [\epsilon_{\theta, \phi^*}(z_t, t, E_t(p), \frac{1}{N-1} \sum_{i=1}^{N-1} \phi^*(h_i^{aux})) - \epsilon_\theta(z_t, t, \emptyset)]. \end{aligned} \quad (17)$$

In practice, we only have to calculate $\phi^*(h^{tar})$ and $\phi^*(h_i^{aux})$ in advance. Then given any character-centric prompt, we can sample images using Eq.17. Also, we can change the guidance scale η_1 and η_2 for an optimal performance.

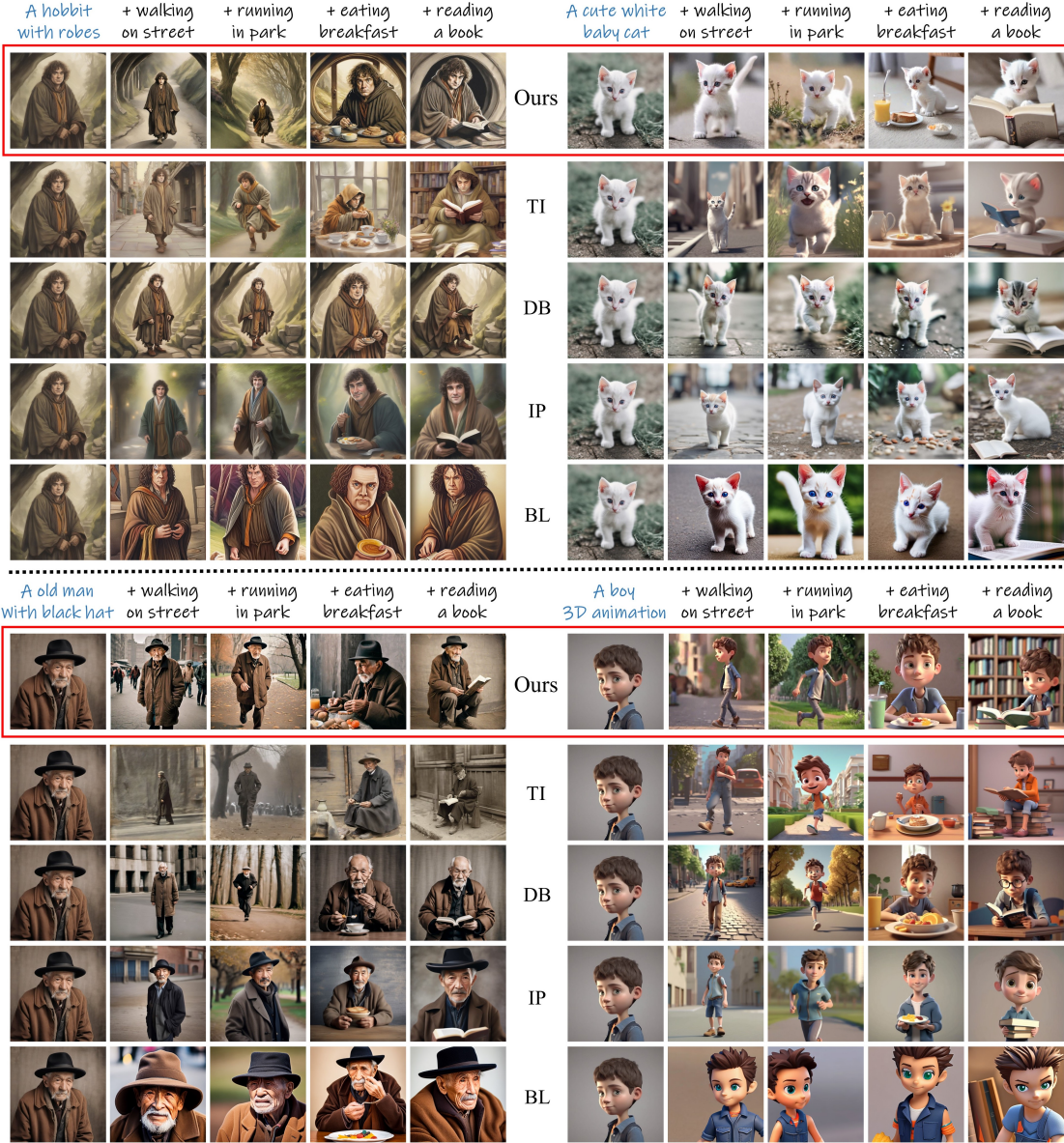


Figure 4: The qualitative comparison between personalization pipelines and our OneActor. Textual Inversion (TI) lacks consistency, while DreamBooth (DB) and IP-Adapter (IP) exhibit limited prompt conformity and diversity. BLIP-Diffusion (BL) suffers from poor quality in certain cases. In contrast, benefiting from the intricate guidance, our OneActor shows superior consistency, diversity as well as stability.

Besides, since our method acts by guiding the latent code to a specific cluster step by step, we can loosen the restrictions by applying cluster guidance to certain steps instead of all steps. Thus, we apply cluster guidance to the early steps while normal guidance to the others to increases the diversity of generated images.

5 Experiments

5.1 Implement Details

We implement our method based on SDXL, which is a common choice by most of the related works. All images are generated in 30 steps. During tuning, we generate $N = 11$ base images. We use $K = 3$ auxiliary images each batch. The projector consists of a 5-layer ResNet and 1 linear layer. The weight hyper-parameters λ_1 and λ_2 are set to 0.5 and

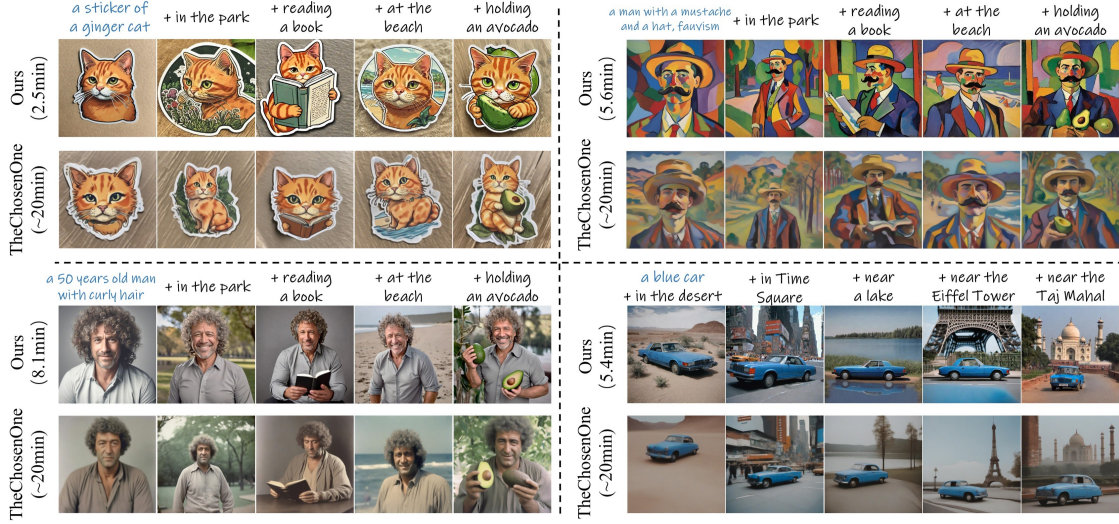


Figure 5: The qualitative comparison between TheChosenOne and our OneActor. Both methods generate consistent and diverse images given different prompts. By comparison, our OneActor refines more details such as the clothes. With 60-85% less tuning time, our OneActor is also much more efficient. Note that we directly quote the results from Avrahami et al. [2023a].

0.3. We tune with a convergence criterion, which takes 3-8 minutes in most cases on a single NVIDIA A100 GPU. During inference, we set the semantic interpolation scale v to 0.8 if not specified. We set the cluster guidance scale η_1 and η_2 to 8.0 and 1.0. We apply cluster guidance to the first 20 inference steps and normal guidance to the last 10 steps.

5.2 Baselines

To evaluate the performance of our method, we compare it with a wide variety of baselines: 1) tuning-based personalization pipeline, Textual Inversion (Gal et al. [2023a]) and DreamBooth (Ruiz et al. [2023]) in a LoRA (Hu et al. [2022]) manner; 2) encoder-based personalization pipeline, IP-Adapter (Ye et al. [2023]) and BLIP-Diffusion (Li et al. [2023]); 3) consistent character generation pipeline, TheChosenOne (Avrahami et al. [2023a]). All of them are applicable in our task setting. For personalization pipeline, we first generate one target image with the given prompt p^tar . Then we use the target image as the input to perform the personalization. For tuning-based pipeline, we tune in the default settings on SDXL. Note that TheChosenOne has not offered an official open-source code, so we compare to the results and illustrations from their written materials.

5.3 Qualitative Evaluation

We illustrate the visual results of personalization baselines and our OneActor in Fig.4. As shown, Textual Inversion generate high-quality and diverse images because it avoids harming the capacity of denoising network. However, its weak tuning method fails to maintain the consistency with the target image. With global tuning, DreamBooth shows, albeit a certain degree of consistency, limited prompt conformity. IP-Adapter maintains consistency in some cases, but is unable to adhere closely to the prompt. BLIP-Diffusion suffers from inferior quality during generation. In contrast, benefiting from the intricate cluster guidance, our OneActor demonstrates a balance of superior character consistency, content diversity as well as prompt conformity. For tuning time, Textual Inversion and DreamBooth take averagely 56 and 62 minutes, respectively. Our OneActor takes 3-8 minutes, which reduces the time by about 90%.

We specifically compare our OneActor with TheChosenOne. For a fair comparison, we quote the images from Avrahami et al. [2023a] and use the same prompts to carry out experiments on our OneActor. The results are shown in Fig.5. Both pipelines manage to generate consistent and diverse images according to the target image. Yet our OneActor preserves more consistent details (e.g. the gray shirt of the man). Moreover, taking tuning time into consideration, TheChosenOne takes an average of 20 minutes while our OneActor only requires averagely 5 minutes. Overall, our method is more efficient and practical.

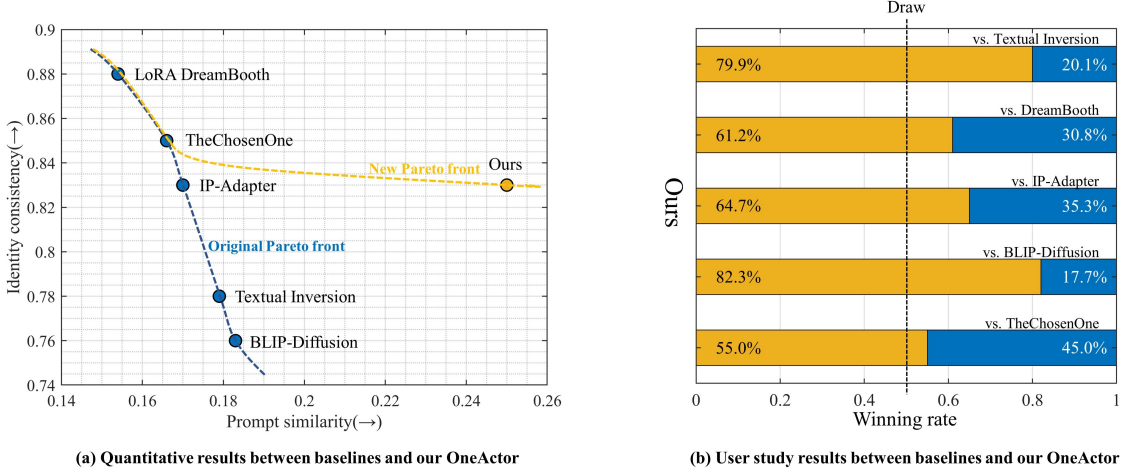


Figure 6: (a) The quantitative comparison between baselines and our OneActor in terms of the identity consistency and the prompt similarity. Our method establishes a new Pareto front with both superior character consistency and prompt conformity. Our method also Pareto dominates IP-Adapter, Textual Inversion and BLIP-Diffusion. (b) The user study results evaluated in terms of character consistency, prompt conformity and content diversity. Our OneActor is more preferred than any baseline. Both quantitative results and user study results correspond with the qualitative results.

5.4 Quantitative Evaluation

To provide an objective assessment, we follow Avrahami et al. [2023a] to carry out quantitative experiments. We collect character target prompts and templates generated by ChatGPT from Avrahami et al. [2023a] for a fair comparison. We use the target prompts to generate target images during tuning. Note that for fairness, we inference with the templates filled with only the base word rather than the whole target prompt because the baselines are designed to function in this way. Our evaluation encompasses 2 dimensions: identity consistency and prompt similarity, which are popular metrics in personalization tasks (Gal et al. [2023a], Ruiz et al. [2023]). Identity consistency is the normalized cosine similarity between the CLIP (Radford et al. [2021]) image embeddings of generated images and that of target image, while the prompt similarity is the similarity between the CLIP text embeddings of the inference prompts and the CLIP image embeddings of the corresponding generated images.

From the results shown in Fig.6(a), we can observe that the baselines originally form a Pareto front. DreamBooth exhibits highest identity consistency at the cost of lowest prompt similarity and diversity. Quite the contrary, Textual Inversion and BLIP-Diffusion sacrifice identity consistency for prompt similarity. TheChosenOne and IP-Adapter form a moderate region with balanced identity consistency and prompt similarity. Now it's time to include our OneActor into the comparison. Since our method makes full use of the capacity of the original diffusion model instead of harming it, it achieves a significant boost of prompt similarity as well as satisfactory identity consistency. Thus, our OneActor establishes a new Pareto front and dominates IP-Adapter, Textual Inversion and BLIP-Diffusion. Generally, the quantitative results correspond to the qualitative results.

5.5 User Study

To provide a subjective assessment, we conduct a user study against the baselines. We build a query webpage and recruit participants to evaluate. Specifically, we follow Podell et al. [2023] and show the participants two sets of images generated from the same target prompt, one by our OneActor and the other by a random baseline. Thus, there are five types of match-ups. We ask participants to choose one preferred set in terms of character consistency, prompt conformity and content diversity. We receive 100 ratings for each match-up, totaling 500 ratings, and illustrate the statistical results in Fig 6(b). As shown, images generated by our method are more preferred than those by any other baseline. These results reveal that, from a human perspective, our method outperforms the baselines.



Figure 7: (a) Illustration of the component ablation study. It shows that every objective component contributes to the enhanced character consistency and content diversity. (b) Illustration of the effect of semantic scale v . We find $v = 0.8$ is optimal because larger v damages the content diversity while smaller v degrades the character consistency. The best results are highlighted with red boxes.

6 Ablation Study

6.1 Component Ablation

The key to our tuning method lies in the three objectives in Sec.4.4. To evaluate the effect of every functional component, we carry out a series of ablation experiments. We start from the original SDXL model and gradually integrate new components, one at a time, to construct three ablating models. We run the process on these four models to obtain character-centric images. For a more intuitive demonstration, we input the same initial noise and prompt to all the models and show the visual results in Fig.7(a). We can observe that, first, with only \mathcal{L}_{tar} , the model can maintain consistency to a certain extent. However, insufficiency of the data causes serious bias issue and damages the diversity of the generated images. Next, including \mathcal{L}_{aux} helps stabilize the tuning and significantly improve the image quality and diversity. Yet the identity consistency is not satisfying. Finally, in the full model, all components add up to function and generate consistent, diverse and high-quality images. The ablation experiments further validate our analysis in Sec.4.2.

6.2 Effect of Semantic Interpolation

We specially add semantic interpolation to enhance the flexibility and controllability during inference in Sec.4.5. To investigate their influence on the generations, we conduct a parameter analysis of semantic scale v . As shown in Fig.7(b), with v increasing, the generated images progressively become more and more consistent with the target image. However, too large v may distort the semantic embeddings and thus damage the content diversity. Hence, we set v to 0.8 for a moderate performance. It's worthy noting that the results correspond with the experiments in Sec.4.5, which proves that the interpolation is feasible to the learned Δc .

7 Conclusion

This paper proposes a new cluster-guided paradigm, OneActor, for consistent character generation. We expect to unleash the internal potential of the ordinary diffusion model using semantic manipulation. Based on the derivation of the cluster-based score function, we design a cluster-conditioned model. During tuning and inference, we utilize several strategies for better performance and efficiency. The experiments in this paper show that: (1) The semantic

space of T2I diffusion models share the same interpolation property as that of the latent space. (2) Benefiting from the intricate guidance, OneActor maintains superior character consistency. (3) Without harming the original model, OneActor demonstrates undegraded image quality and prompt conformity. (4) OneActor requires an average tuning time of 5 minutes, at least 4 \times faster than the baselines.

References

Jonathan Ho, Ajay Jain, and Pieter Abbeel. Denoising diffusion probabilistic models. In Hugo Larochelle, Marc'Aurelio Ranzato, Raia Hadsell, Maria-Florina Balcan, and Hsuan-Tien Lin, editors, *Advances in Neural Information Processing Systems 33: Annual Conference on Neural Information Processing Systems 2020, NeurIPS 2020, December 6-12, 2020, virtual*, 2020. URL <https://proceedings.neurips.cc/paper/2020/hash/4c5bcfec8584af0d967f1ab10179ca4b-Abstract.html>.

Dustin Podell, Zion English, Kyle Lacey, Andreas Blattmann, Tim Dockhorn, Jonas Müller, Joe Penna, and Robin Rombach. SDXL: improving latent diffusion models for high-resolution image synthesis. *CoRR*, abs/2307.01952, 2023. doi:10.48550/ARXIV.2307.01952. URL <https://doi.org/10.48550/arXiv.2307.01952>.

Rinon Gal, Yuval Alaluf, Yuval Atzmon, Or Patashnik, Amit Haim Bermano, Gal Chechik, and Daniel Cohen-Or. An image is worth one word: Personalizing text-to-image generation using textual inversion. In *The Eleventh International Conference on Learning Representations, ICLR 2023, Kigali, Rwanda, May 1-5, 2023*. OpenReview.net, 2023a. URL <https://openreview.net/pdf?id=NAQvF08TcyG>.

Nataniel Ruiz, Yuanzhen Li, Varun Jampani, Yael Pritch, Michael Rubinstein, and Kfir Aberman. Dreambooth: Fine tuning text-to-image diffusion models for subject-driven generation. In *IEEE/CVF Conference on Computer Vision and Pattern Recognition, CVPR 2023, Vancouver, BC, Canada, June 17-24, 2023*, pages 22500–22510. IEEE, 2023. doi:10.1109/CVPR52729.2023.02155. URL <https://doi.org/10.1109/CVPR52729.2023.02155>.

Hu Ye, Jun Zhang, Sibo Liu, Xiao Han, and Wei Yang. Ip-adapter: Text compatible image prompt adapter for text-to-image diffusion models. *CoRR*, abs/2308.06721, 2023. doi:10.48550/ARXIV.2308.06721. URL <https://doi.org/10.48550/arXiv.2308.06721>.

Yuxiang Wei, Yabo Zhang, Zhilong Ji, Jinfeng Bai, Lei Zhang, and Wangmeng Zuo. ELITE: encoding visual concepts into textual embeddings for customized text-to-image generation. In *IEEE/CVF International Conference on Computer Vision, ICCV 2023, Paris, France, October 1-6, 2023*, pages 15897–15907. IEEE, 2023. doi:10.1109/ICCV51070.2023.01461. URL <https://doi.org/10.1109/ICCV51070.2023.01461>.

Adyasha Maharana, Darryl Hannan, and Mohit Bansal. Storydall-e: Adapting pretrained text-to-image transformers for story continuation. In Shai Avidan, Gabriel J. Brostow, Moustapha Cissé, Giovanni Maria Farinella, and Tal Hassner, editors, *Computer Vision - ECCV 2022 - 17th European Conference, Tel Aviv, Israel, October 23-27, 2022, Proceedings, Part XXXVII*, volume 13697 of *Lecture Notes in Computer Science*, pages 70–87. Springer, 2022. doi:10.1007/978-3-031-19836-6_5. URL https://doi.org/10.1007/978-3-031-19836-6_5.

Tanzila Rahman, Hsin-Ying Lee, Jian Ren, Sergey Tulyakov, Shweta Mahajan, and Leonid Sigal. Make-a-story: Visual memory conditioned consistent story generation. In *IEEE/CVF Conference on Computer Vision and Pattern Recognition, CVPR 2023, Vancouver, BC, Canada, June 17-24, 2023*, pages 2493–2502. IEEE, 2023. doi:10.1109/CVPR52729.2023.00246. URL <https://doi.org/10.1109/CVPR52729.2023.00246>.

Omri Avrahami, Amir Hertz, Yael Vinker, Moab Arar, Shlomi Fruchter, Ohad Fried, Daniel Cohen-Or, and Dani Lischinski. The chosen one: Consistent characters in text-to-image diffusion models. *arXiv preprint arXiv:2311.10093*, 2023a.

Yael Vinker, Andrey Voynov, Daniel Cohen-Or, and Ariel Shamir. Concept decomposition for visual exploration and inspiration. *ACM Trans. Graph.*, 42(6):241:1–241:13, 2023. doi:10.1145/3618315. URL <https://doi.org/10.1145/3618315>.

Omri Avrahami, Kfir Aberman, Ohad Fried, Daniel Cohen-Or, and Dani Lischinski. Break-a-scene: Extracting multiple concepts from a single image. In June Kim, Ming C. Lin, and Bernd Bickel, editors, *SIGGRAPH Asia 2023 Conference Papers, SA 2023, Sydney, NSW, Australia, December 12-15, 2023*, pages 96:1–96:12. ACM, 2023b. doi:10.1145/3610548.3618154. URL <https://doi.org/10.1145/3610548.3618154>.

Yuval Alaluf, Elad Richardson, Gal Metzer, and Daniel Cohen-Or. A neural space-time representation for text-to-image personalization. *ACM Trans. Graph.*, 42(6):243:1–243:10, 2023. doi:10.1145/3618322. URL <https://doi.org/10.1145/3618322>.

Ligong Han, Yinxiao Li, Han Zhang, Peyman Milanfar, Dimitris N. Metaxas, and Feng Yang. Svdiff: Compact parameter space for diffusion fine-tuning. In *IEEE/CVF International Conference on Computer Vision, ICCV 2023*,

Paris, France, October 1-6, 2023, pages 7289–7300. IEEE, 2023. doi:10.1109/ICCV51070.2023.00673. URL <https://doi.org/10.1109/ICCV51070.2023.00673>.

Nupur Kumari, Bingliang Zhang, Richard Zhang, Eli Shechtman, and Jun-Yan Zhu. Multi-concept customization of text-to-image diffusion. In *IEEE/CVF Conference on Computer Vision and Pattern Recognition, CVPR 2023, Vancouver, BC, Canada, June 17-24, 2023*, pages 1931–1941. IEEE, 2023. doi:10.1109/CVPR52729.2023.00192. URL <https://doi.org/10.1109/CVPR52729.2023.00192>.

Yoad Tewel, Rinon Gal, Gal Chechik, and Yuval Atzmon. Key-locked rank one editing for text-to-image personalization. In Erik Brunvand, Alla Sheffer, and Michael Wimmer, editors, *ACM SIGGRAPH 2023 Conference Proceedings, SIGGRAPH 2023, Los Angeles, CA, USA, August 6-10, 2023*, pages 12:1–12:11. ACM, 2023. doi:10.1145/3588432.3591506. URL <https://doi.org/10.1145/3588432.3591506>.

Rinon Gal, Moab Arar, Yuval Atzmon, Amit H. Bermano, Gal Chechik, and Daniel Cohen-Or. Encoder-based domain tuning for fast personalization of text-to-image models. *ACM Trans. Graph.*, 42(4):150:1–150:13, 2023b. doi:10.1145/3592133. URL <https://doi.org/10.1145/3592133>.

Wenhu Chen, Hexiang Hu, Yandong Li, Nataniel Ruiz, Xuhui Jia, Ming-Wei Chang, and William W. Cohen. Subject-driven text-to-image generation via apprenticeship learning. In Alice Oh, Tristan Naumann, Amir Globerson, Kate Saenko, Moritz Hardt, and Sergey Levine, editors, *Advances in Neural Information Processing Systems 36: Annual Conference on Neural Information Processing Systems 2023, NeurIPS 2023, New Orleans, LA, USA, December 10 - 16, 2023*, 2023. URL http://papers.nips.cc/paper_files/paper/2023/hash/6091bf1542b118287db4088bc16be8d9-Abstract-Conference.html.

Moab Arar, Rinon Gal, Yuval Atzmon, Gal Chechik, Daniel Cohen-Or, Ariel Shamir, and Amit H. Bermano. Domain-agnostic tuning-encoder for fast personalization of text-to-image models. In June Kim, Ming C. Lin, and Bernd Bickel, editors, *SIGGRAPH Asia 2023 Conference Papers, SA 2023, Sydney, NSW, Australia, December 12-15, 2023*, pages 72:1–72:10. ACM, 2023. doi:10.1145/3610548.3618173. URL <https://doi.org/10.1145/3610548.3618173>.

Jonathan Ho and Tim Salimans. Classifier-free diffusion guidance. *CoRR*, abs/2207.12598, 2022. doi:10.48550/ARXIV.2207.12598. URL <https://doi.org/10.48550/arXiv.2207.12598>.

Xulu Zhang, Xiao-Yong Wei, Jinlin Wu, Tianyi Zhang, Zhaoxiang Zhang, Zhen Lei, and Qing Li. Compositional inversion for stable diffusion models. In Michael J. Wooldridge, Jennifer G. Dy, and Sriraam Natarajan, editors, *Thirty-Eighth AAAI Conference on Artificial Intelligence, AAAI 2024, Thirty-Sixth Conference on Innovative Applications of Artificial Intelligence, IAAI 2024, Fourteenth Symposium on Educational Advances in Artificial Intelligence, EAAI 2024, February 20-27, 2024, Vancouver, Canada*, pages 7350–7358. AAAI Press, 2024. doi:10.1609/AAAI.V38I7.28565. URL <https://doi.org/10.1609/aaai.v38i7.28565>.

Gaurav Parmar, Krishna Kumar Singh, Richard Zhang, Yijun Li, Jingwan Lu, and Jun-Yan Zhu. Zero-shot image-to-image translation. In Erik Brunvand, Alla Sheffer, and Michael Wimmer, editors, *ACM SIGGRAPH 2023 Conference Proceedings, SIGGRAPH 2023, Los Angeles, CA, USA, August 6-10, 2023*, pages 11:1–11:11. ACM, 2023. doi:10.1145/3588432.3591513. URL <https://doi.org/10.1145/3588432.3591513>.

Thao Nguyen, Yuheng Li, Utkarsh Ojha, and Yong Jae Lee. Visual instruction inversion: Image editing via image prompting. In Alice Oh, Tristan Naumann, Amir Globerson, Kate Saenko, Moritz Hardt, and Sergey Levine, editors, *Advances in Neural Information Processing Systems 36: Annual Conference on Neural Information Processing Systems 2023, NeurIPS 2023, New Orleans, LA, USA, December 10 - 16, 2023*, 2023. URL http://papers.nips.cc/paper_files/paper/2023/hash/1e75f7539cbde5de895fab238ff42519-Abstract-Conference.html.

Jascha Sohl-Dickstein, Eric A. Weiss, Niru Maheswaranathan, and Surya Ganguli. Deep unsupervised learning using nonequilibrium thermodynamics. In Francis R. Bach and David M. Blei, editors, *Proceedings of the 32nd International Conference on Machine Learning, ICML 2015, Lille, France, 6-11 July 2015*, volume 37 of *JMLR Workshop and Conference Proceedings*, pages 2256–2265. JMLR.org, 2015. URL <http://proceedings.mlr.press/v37/sohl-dickstein15.html>.

Olaf Ronneberger, Philipp Fischer, and Thomas Brox. U-net: Convolutional networks for biomedical image segmentation. In Nassir Navab, Joachim Hornegger, William M. Wells III, and Alejandro F. Frangi, editors, *Medical Image Computing and Computer-Assisted Intervention - MICCAI 2015 - 18th International Conference Munich, Germany, October 5 - 9, 2015, Proceedings, Part III*, volume 9351 of *Lecture Notes in Computer Science*, pages 234–241. Springer, 2015. doi:10.1007/978-3-319-24574-4_28. URL https://doi.org/10.1007/978-3-319-24574-4_28.

Robin Rombach, Andreas Blattmann, Dominik Lorenz, Patrick Esser, and Björn Ommer. High-resolution image synthesis with latent diffusion models. In *IEEE/CVF Conference on Computer Vision and Pattern Recognition, CVPR 2022, New Orleans, LA, USA, June 18-24, 2022*, pages 10674–10685. IEEE, 2022. doi:10.1109/CVPR52688.2022.01042. URL <https://doi.org/10.1109/CVPR52688.2022.01042>.

Yang Song, Jascha Sohl-Dickstein, Diederik P. Kingma, Abhishek Kumar, Stefano Ermon, and Ben Poole. Score-based generative modeling through stochastic differential equations. In *9th International Conference on Learning Representations, ICLR 2021, Virtual Event, Austria, May 3-7, 2021*. OpenReview.net, 2021. URL <https://openreview.net/forum?id=PxTIG12RRHS>.

Kaiming He, Xiangyu Zhang, Shaoqing Ren, and Jian Sun. Deep residual learning for image recognition. In *2016 IEEE Conference on Computer Vision and Pattern Recognition, CVPR 2016, Las Vegas, NV, USA, June 27-30, 2016*, pages 770–778. IEEE Computer Society, 2016. doi:10.1109/CVPR.2016.90. URL <https://doi.org/10.1109/CVPR.2016.90>.

Edward J. Hu, Yelong Shen, Phillip Wallis, Zeyuan Allen-Zhu, Yuanzhi Li, Shean Wang, Lu Wang, and Weizhu Chen. Lora: Low-rank adaptation of large language models. In *The Tenth International Conference on Learning Representations, ICLR 2022, Virtual Event, April 25-29, 2022*. OpenReview.net, 2022. URL <https://openreview.net/forum?id=nZeVKeeFYf9>.

Dongxu Li, Junnan Li, and Steven C. H. Hoi. Blip-diffusion: Pre-trained subject representation for controllable text-to-image generation and editing. In Alice Oh, Tristan Naumann, Amir Globerson, Kate Saenko, Moritz Hardt, and Sergey Levine, editors, *Advances in Neural Information Processing Systems 36: Annual Conference on Neural Information Processing Systems 2023, NeurIPS 2023, New Orleans, LA, USA, December 10 - 16, 2023*, 2023. URL http://papers.nips.cc/paper_files/paper/2023/hash/602e1a5de9c47df34cae39353a7f5bb1-Abstract-Conference.html.

Alec Radford, Jong Wook Kim, Chris Hallacy, Aditya Ramesh, Gabriel Goh, Sandhini Agarwal, Girish Sastry, Amanda Askell, Pamela Mishkin, Jack Clark, Gretchen Krueger, and Ilya Sutskever. Learning transferable visual models from natural language supervision. In Marina Meila and Tong Zhang, editors, *Proceedings of the 38th International Conference on Machine Learning, ICML 2021, 18-24 July 2021, Virtual Event*, volume 139 of *Proceedings of Machine Learning Research*, pages 8748–8763. PMLR, 2021. URL <http://proceedings.mlr.press/v139/radford21a.html>.